ISIJ International, Vol. 44 (2004), No. 5, pp. 869–877

Influence of the Geometry of an Immersed Steel Workpiece on Mass Transfer Coefficient in a Chemical Heat Treatment Fluidised Bed

Weimin GAO, John M. LONG, Lingxue KONG[1)] and Peter D. HODGSON

School of Engineering and Technology, Deakin University, Geelong, Vic.3217, Australia.
1) Centre for Advanced Manufacturing and Research, University of South Australia, Mawson Lakes, SA 5095, Australia.

(*Received on February 24, 2003; accepted in final form on January 27, 2004*)

The mass transfer during carburising in a fluidised bed and in a steel workpiece has been studied experimentally in this work. This involved carburising experiment in an electrically heated fluidised bed at 900–970°C with natural gas and air as the atmosphere. A steel workpiece was designed to provide a range of carbon transfer surfaces of different geometries in the fluidised bed, and the carbon transfer coefficient was measured at these surfaces. The carbon transfer coefficient was determined from the carbon distribution within the diffusion layer of the sample. An empirical relationship of the carbon potential as a function of carburising atmosphere, bed temperature and fluidising velocity was determined, based on the understanding of the mass transfer mechanism and analysis of the experimental results.

KEY WORDS: fluidised bed; mass transfer; carburising; heat treatment.

1. Introduction

The fluidised bed furnace has widely been used in the heat treatment of metals. There can be a number of advantages in using fluidised bed technology in the surface modification of steels in processes such as: carburising, carbonitriding, nitriding, and nitrocarburizing.[1–7)] Each technique is a process of mass transfer from the bed to the surface of a steel workpiece. Even though a number of heat treatment techniques have been developed for different purposes,[8–11)] there have been few studies of the mass transfer mechanism and the relationship between fluidising parameters and the mass transfer coefficient.[5,12)] It is necessary to know the effect of operation parameters on mass transfer to understand the mass transfer mechanism in the fluidised bed and to optimise the benefits and control the heat treatment process.

In this paper, a carburising experiment was performed in an electrically heated fluidised bed furnace with temperatures from 900–970°C, using natural gas and air. The carbon transfer coefficient was extracted from the carbon distribution within treated layer. An empirical relationship between carbon transfer coefficient and carbon potential of carburising atmosphere, bed temperature and fluidising velocity was developed and the mass transfer mechanism was analysed.

2. Principles

The carbon transfer theory in a fluidised bed is based on the assumption of carbon transfer by gas–solid dense groups (emulsion phase), that are periodically removed from the carbon transfer surface by carburising gas bubbles (bubble phase). The carbon transfer is achieved by the movement of the emulsion, which carries the carburising gases from the bed to the carbon transfer surface, and then by chemical reactions on the carbon transfer surface.

When natural gas is used to enrich the carburising process, the main reactions on carbon transfer surface consist of:

$$2CO \rightarrow [C] + CO_2 \quad \text{.....(1)}$$

$$CO + H_2 \rightarrow [C] + H_2O \quad \text{.....(2)}$$

$$CH_4 \rightarrow [C] + 2H_2 \quad \text{.....(3)}$$

The mechanisms of reactions of Eqs. (1) and (2) can be described as the process of absorption of CO (Eq. (4)), and the desorption of adsorbed oxygen atom by CO and H_2 (Eqs. (5) and (6)).

$$CO \rightarrow C_{ad} + O_{ad} \quad \text{.....(4)}$$

$$H_2 + O_{ad} \rightarrow H_2O \quad \text{.....(5)}$$

$$CO + O_{ad} \rightarrow CO_2 \quad \text{.....(6)}$$

Different carbon transfer mechanisms have been proposed for controlling the rate in conventional gas carburising. Meschter and Kaspersma reported that the reaction of CO or H_2 and the oxygen absorbed on the steel surface determines the carburising process.[13,14)] Fruehan pointed out that the activated complex on a carbon transfer surface is important in controlling the transfer rate.[15)] Ling *et al.*[16)] used a critical coverage of absorbed oxygen to determine which reaction controls the carbon transfer process. Dragomir *et*

al. summarised the reaction rates in the literature and produced a total carbon transfer coefficient without studying the difference in the order of magnitude of reactions (1)–(3).[12]

Actually, reaction rate of Eq. (5) is only 1/10 of reaction rate of Eq. (4) and the H_2 content is much higher than the CO content when air and rich natural gas are used as the carburising agent in fluidised beds. The chemical reaction rate is controlled by the absorption of CO in fluidised beds and was given by,[16]

$$v=\frac{k_4'k_5'P_{H_2O}}{k_5P_{H_2}}\left(\frac{K_4K_5P_{H_2}P_{CO}}{P_{H_2O}}-a_c-K_4P_{CO}\right) \quad \text{.....(7)}$$

Taking into account of the carbon activity, $a_{g,1}=K_4K_5P_{H_2}P_{CO}/P_{H_2O}$, Eq. (7) can be written,

$$v=\beta_{CO}(a_{g,1}-a_c) \quad \text{.....(8)}$$

The carbon transfer coefficient for this reaction is,

$$\beta_{CO}=\frac{k_4'k_5'P_{H_2O}}{k_5P_{H_2}}\left(1-\frac{K_4P_{CO}}{a_{g,1}-a_c}\right) \quad \text{.....(9)}$$

The mechanism of carbon transferred from CH_4 to the steel surface was investigated.[17] He proposed that during carburising in mixtures of CH_4–H_2, the reaction is composed by the following reaction sequence:

$$CH_4\rightarrow CH_{4ad}\rightarrow CH_{3ad}+H_{ad}\rightarrow CH_{2ad}+2H_{ad}$$
$$\rightarrow CH_{ad}+3H_{ad}\rightarrow C_{ad}+4H_{ad}\rightarrow C_\gamma+2H_2$$

The rate of the forward reaction is proportional to $P_{CH_4}/P_{H_2}^{1/2}$ and the rate of the backward reaction is proportional to $P_{H_2}^{3/2}$. Then, the reaction rate of Eq. (3) is,

$$v=k_3\frac{P_{CH_4}}{P_{H_2}^{1/2}}-k_3'a_cP_{H_2}^{3/2} \quad \text{.....(10)}$$

Considering $K_3=k_3/k_3'$ and the carbon activity in the H_2–CH_4 is $a_{g,2}=K_3P_{CH_4}/P_{H_2}^2$, the Eq. (10) becomes,

$$v=\beta_{CH_4}(a_{g,2}-a_c) \quad \text{.....(11)}$$

and the carbon transfer coefficient for this reaction is

$$\beta_{CH_4}=k_3'P_{H_2}^{3/2} \quad \text{.....(12)}$$

Gas carburising in fluidised beds is a nonequilibrium process. The gaseous constituents of the atmosphere are not fully in equilibrium with the steel being carburised and are controlled by the behaviour of the bubble and emulsion phases and by the complex interactions of the gaseous species. Such as

$$CO+H_2O\leftrightarrow CO_2+H_2 \quad \text{.....(13)}$$

$$CH_4+CO_2\rightarrow H_2+2CO \quad \text{.....(14)}$$

$$CH_4+H_2O\rightarrow 3H_2+CO \quad \text{.....(15)}$$

The methane enrichment of the endothermic gas provides carbon for the process by slow reactions, such as reactions of Eqs. (14) and (15), which reduce the concentration of CO_2 and H_2O. These reactions regenerate CO and H_2, thereby directing the reactions of Eqs. (1) and (2) to the right. Because the methane content of the carburising atmosphere is usually far above the content that is expected at equilibrium, reaction of Eq. (3) becomes important in the carbon transfer rate.

Most of the rich methane is actually cracked without touching the steel and is turned to soot, resulting in deposited soot inside the surfaces of fluidising particles, workpiece and furnace. The fluidising particles carry the generated soot to the zone near the bottom of the bed, where amounts of H_2O and CO_2 exist. The soot reacts with H_2O and CO_2 and generates CO and H_2, raising the carbon potential of the carburising atmosphere.

Therefore, the carbon transfer from fluidised beds to the workpiece can be represented as in Fig. 1 and involves the following steps:

1. Formation of a carburising atmosphere;
2. Transport of the molecules in the boundary layer. Those containing carbon (CO, CH_4 *etc.*) transport through the carburising atmosphere to the steel surface, but other oxidise gases (CO_2, H_2O) from the steel surface;
3. Diffusion of the molecules that contain carbon (CO, CH_4) through the Nernst layer and adsorption on the steel surface;
4. Decomposition of the molecules adsorbed at the gaseous atmosphere/steel surface interface;
5. Adsorption of the carbon atoms and desorption of the oxygen atoms absorbed on the steel surface; and
6. Dissolution of carbon atom on the steel surface and diffusion in the steel.

The carbon concentration is divided into three regimes. The difference (C_p-C_p'), between the carbon concentration, C_p which characterises the carbon activity of carburising gases in the fluidised bed and the carbon potential, C_p' indicating the carbon activity from the composition of the gaseous species at the steel surface, is governed by fluidising hydrodynamics and the reaction of species in the phase boundary. The difference $(C_p'-C_s)$ between the carbon potential on the steel surface and the carbon concentration at the steel surface, C_s, is controlled by the reaction of the absorption and decomposition of the carburising molecules and the desorption of oxygen atoms at the steel surface. The difference (C_s-C_0) between the surface carbon con-

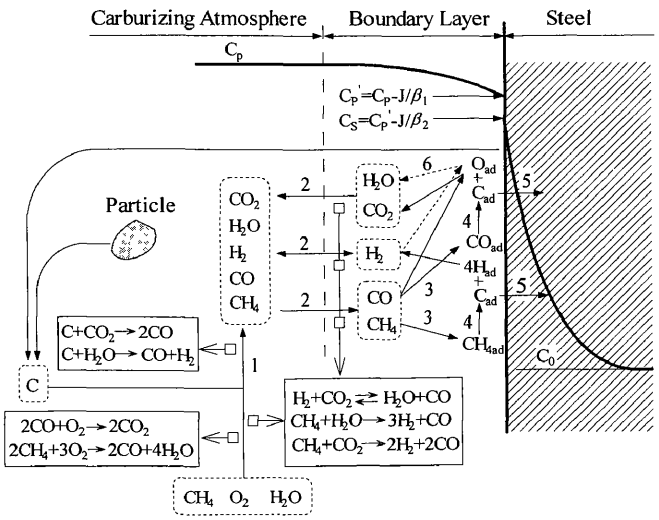

Fig. 1. The carbon transfer mechanism.

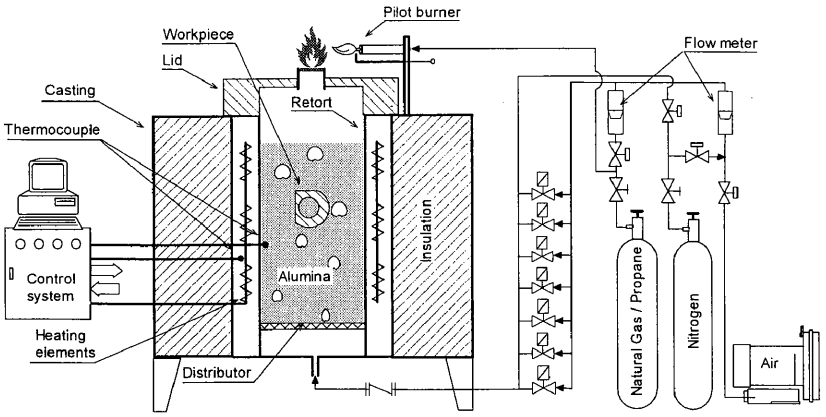

Fig. 2. The schematic diagram of the fluidised bed furnace.

centration and the core carbon concentration drives the carbon diffusion within the steel. The carbon transfer coefficients, β_1 and β_2, representing these two regimes of $(C_p - C'_p)$ and $(C'_p - C_s)$, are also shown in **Fig. 1**.

The carbon transfer rate at the steel surface is determined by steps 2 to 5 at the start of the carburising process. After the carbon concentration in the steel surface reaches a certain value, the diffusion inside the steel, step 6, mainly controls the carbon transfer processes, specifically in the process of the boost and diffuse carburising technology. In step 2, the carbon transfer rate in the boundary layer depends on the rate of diffusion of the carburising gas from the gas–solid groups and on the frequency of their replacement at the surface. The reaction rate in steps 3–5 depends on the chemical activity of the gases, the carbon potential of the atmosphere and the carburising temperature, in addition to the fluidising parameters such as fluidising velocity, fluidising particle and gas properties, and bubble fraction, *etc.*

3. Experimental Facilities

3.1. Fluidised Bed

A commercial electrically heated fluidised bed furnace, designed for metal heat treatment was used for the purpose of this work. This is shown schematically in **Fig. 2** and the specifications are given in **Table 1**.

The furnace and structure is fabricated from steel and enclosed in a sheet metal casing. The casing is lined with layers of ceramic fibre insulation. In the centre of the furnace is the retort fitted with an air distributor in the base. Surrounding the retort are three silicon–carbon heating elements, which slot into support plates at the base of the furnace. Power to the elements is controlled by thyristor in the electrical control panel, which in turn receives its signal from a Shinko temperature controller. This controller also ensures that reactive gases only enter the furnace above a specified temperature. Also provided is a Novatech MC-71 over-temperature controller which cuts power to the elements should the temperature exceed a preset value. All operations are carried out on the control panel. A computer control system connected with the controller is also provided to run the furnace.

Natural gas controlled by two flow meters with scales of 3.0 m^3/h and 1.0 m^3/h and air provided by the air blower

Table 1. The specifications of the fluidised bed.

Name	Specifications
Working chamber size	200mm diameter×400mm deep
External casing	600mm diameter, 3mm mild steel plate
Insulation	200mm ceramic fibre wool
Retort material	Inconel 601
Retort distributor	316 stainless steel sintered discs
Rated power supply	18kW (425V, 3phase, 50Hz)
Heating elements	Silicon carbide (U20×350×250-50)
Fluidising medium	Alumina of 120mesh
Max. working temperature	1180 °C
Temperature uniformity	±5 °C
Fluidisation gases	Air and Nitrogen
Reactive gases	Propane, Natural gas and Ammonia

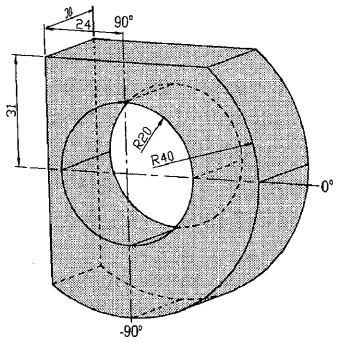

Fig. 3. Design of workpiece (unit: mm).

(ELMO gas ring vacuum compressor from Siemens) were mixed as the carburising agent and are used to fluidise the bed. Nitrogen from a purity cylinder was available as an inter gas for fluidising bed above 600°C to prevent oxidation of the metal workpiece. A 0.0–7.0 m^3/h M-Type flow meter (Waukee Engineering CO., Inc.) was used to control and measure the air or nitrogen rates. Connected in series with the flow meter were seven parallel lines with solenoid values used to adjust the volume of the fluidising gases automatically and limit the gas rate to run the furnace at the fluidising number of less than 4.2, because of safety. An exceedingly fluidising velocity would cause the spilling of the hot fluidising particles out of the furnace. The maximum gas rate varied with the bed temperature on the relationship of gas expansion and temperature. All the gas supplies and associated values were computer controlled.

The effluent gases from the top of fluidised bed were burned by a pilot burner.

3.2. Workpiece and Steel Sheet

This work employed a steel workpiece with a carbon

content of 0.05% as shown in **Fig. 3**. The orientation of workpiece positioned in the fluidised bed is shown in Fig. 2. The various flat and curved surfaces present some possible mass transfer position in fluidised beds to different product geometries. The contact between workpiece surfaces was simulated by immersing two or three workpieces, which leaned against each other and were aligned along the axis of the circle, in the bed, as well as the effect of workpiece size was considered.

The carbon potential of the bed was estimated by carburising a low carbon steel sheet of 0.1–0.15 mm thick and 20×60 mm in area and measuring its carbon depth profile.

3.3. Test Conditions and Procedures

Only 120-mesh alumina was used as the fluidising medium in this work. The particle density and bulk density of the bed were 3 890 and 1 830 kg/m^3, respectively. The particles can be classified as Geldart[18] group B under ambient conditions in air. The minimum fluidising velocity, U_{mf}, of 0.022 m/s was developed after measuring the gas pressure drop through the bed.

The carburising atmosphere was natural gas plus air. The air/natural gas ratio was in the range of 1.33–8.34, with a fluidising velocity of $2.47U_{mf}$ and the bed temperature of 910°C, 930°C, 950°C and 970°C was selected. These were chosen to determine the carbon potential at the given air/natural gas and bed temperature, and establish a relationship of the carbon transfer coefficient to the bed temperature and the carbon potential. The experiment was carried out for different fluidising velocities to investigate this effect on the carbon transfer coefficient. The carbon transfer coefficient was measured at the front/back vertical surface of workpiece shown in Fig. 3. It was also measured at different positions on the workpiece surface for some of the above cases to investigate the local heat transfer coefficient around the workpiece.

Prior to carburising, an initial heating process of 15 min in nitrogen fluidisation was applied to increase the temperature of workpiece to the test temperature. After this the gas was introduced for a specified time and then the workpiece was quenched in water. Subsequently, the carbon distribution within treated layer of workpiece was analyzed by a LECO-GDS850A glow-discharge optical emission spectrometer (GDOES). Because the maximum depth sputtered by GDOES is about 100 μm, the sputtered hole or layer must be ground off to test carbon in further depth. It is highly important to grind the samples to remove the sputtered layer uniformly for reaching a precise carbon variation with depth. Several grinds and burns were necessary to measure the carbon distribution within the diffusion layer of about 1.00 mm in depth. Generally, the ground layers were a little thicker than those sputtered layers to reduce the times of the grinding and sputtering on the precondition of getting the carbon distribution within the diffusion layer. The treatment cycle is shown in **Fig. 4**.

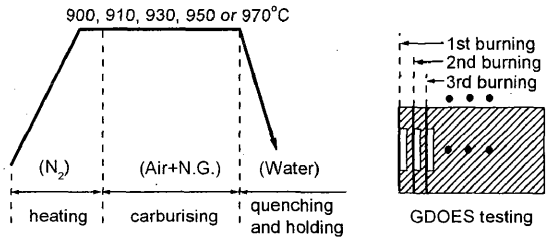

Fig. 4. Carburising procedure and measurement.

4. Extraction of the Mass Transfer Coefficient and Diffusivity

The distribution of the carbon concentration within treated layer can be calculated by using the following formula, which is the analytical solution of the mass transfer differential equations.[19]

$$\frac{C-C_0}{C_p-C_0}=\mathrm{erfc}\left(\frac{x}{2\sqrt{Dt}}\right)-\exp\left(\frac{\beta x+\beta^2 t}{D}\right)\mathrm{erfc}\left(\frac{x}{2\sqrt{Dt}}+\frac{\beta\sqrt{t}}{\sqrt{D}}\right) \quad \text{....(16)}$$

Theoretically, the value of carbon concentration, C, at one position, x, within the treated layer is sufficient to calculate the mass transfer coefficient, β, with the above formula, if the carbon diffusivity within steel, D, is available. At present, though the diffusivity of most alloy steels is not well documented. It must be determined at the time of measuring the mass transfer coefficient. Therefore, the carbon distribution within the treated layer is required to calculate β and D simultaneously.

The carbon transfer coefficient, β, at the immersed surface and the carbon diffusivity, D, within steel can be determined by fitting the experimental data with the above formula. The Levenberg–Marquardt algorithm was used to fit the data. In order to increase the precision, the experiment was carried out with different carburising times and the sum of the mean squared errors (MSEs) was used to optimise the parameters.

Figure 5 shows the carbon distribution within workpiece after a carburising time of 10 min, 30 min and 60 min, with a fluidising velocity of $2.47U_{mf}$, a carbon potential of 1.43%, and a bed temperature of 930°C, as well as the results of the regression and the fitted curves. In all cases the curve fitting is very accurate although it is less accurate for 60 min than that for 10 and 30 min. For 60 min, the carbon concentrations within the treated layer are higher than the corresponding fitted values except towards the specimen

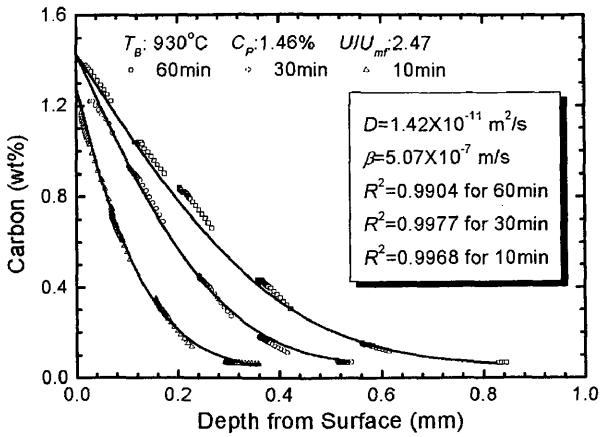

Fig. 5. Carbon distribution within workpiece.

centre. This is caused by the assumption of a constant carbon diffusivity, D, in Eq. (10). However, the diffusivity of carbon within steel actually increases with an increase in the carbon concentration.[20] At this time the carbon transfer distribution within steel is mainly determined by the carbon diffusion within steel. The effect of the carbon transfer flux at the workpiece surface on the carbon distribution is significantly reduced. Hence the correct selection of the carburising time is important in determining the carbon transfer coefficient and the carbon diffusivity by fitting the experimental data with Eq. (16) to investigate the effect of fluidising and carburising parameters (such as carbon potential, bed temperature, fluidising velocity, *etc.*) on the carbon transfer coefficient. The experiment should be taken before the time in which the carbon transfer flux is mainly controlled by the carbon diffusion inside the steel. However, carburising in too short a time does not provide enough data to achieve high accuracy in the regression. In the present experiment, a reasonable carburising time was in the range of 10–30 min.

The diffusivities of carbon in this steel at 900°C, 910°C, 950°C and 970°C were also extracted by using the same method. Once the diffusivity was determined, the carbon transfer coefficient was calculated from the data of the first GDOES burn.

5. Results and Discussion

5.1. Carbon Potential and Bed Temperature

The carbon potential of the carburising atmosphere, a measure of the atmosphere containing active carbon to alter or maintain the carbon level of the steel, is required to be higher than the carbon content of the workpiece to be carburised. The higher activity of carbon in the carburising atmosphere than in the steel leads a difference, $(a_g - a_c)$ in Eqs. (8) and (11), provides a driving force for carbon transfer to the workpiece. Meanwhile, it is the atmosphere composition, which is the function of the carbon potential, that determines the carbon transfer coefficient at the specified temperature and fluidising condition, as shown in Eqs. (9) and (12). The temperature affects not only the diffusion of carbon in austenite also the reaction rate at the surface of the workpiece. Therefore, the surface carbon transfer coefficient, β, is particularly dependent on the carbon potential, C_p, of the carburising atmosphere and the carburising temperature.

Figure 6 shows that the carbon transfer coefficient on the vertical surface increases with an increase in carbon potential and temperature. The results have been analysed to show the relationship between carbon potential, temperature and carbon transfer coefficient (**Fig. 7**). The equation:

$$\beta = (a_1 + a_2 C_p^n) \exp\left(-\frac{Q}{RT}\right) \quad \text{.....(17)}$$

shows a exponential dependence of the carbon transfer coefficient on the carbon potential and an activation energy relationship between the carbon transfer coefficient and temperature. The power, n, of 6.22 obtained in the current experiments (Fig. 7) implies a strong dependence of the carbon transfer coefficient on the carbon potential. For conventional gas carburising, the dependence has been reported by Neumann and Wyss with a relationship of the carbon transfer coefficient to the composition of the carburising atmosphere.[21] They found that β increases with an increase in the sum of CH_4, H_2 and H_2O contents, which is the function of the carbon potential at a specified temperature, when the sum of their contents is lower than 50%.

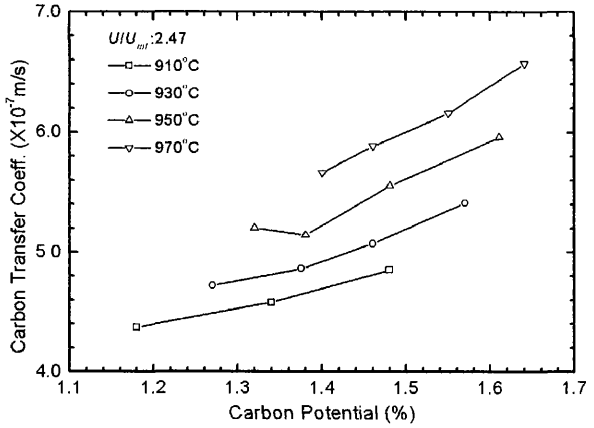

Fig. 6. Variation of β with C_b and T_b.

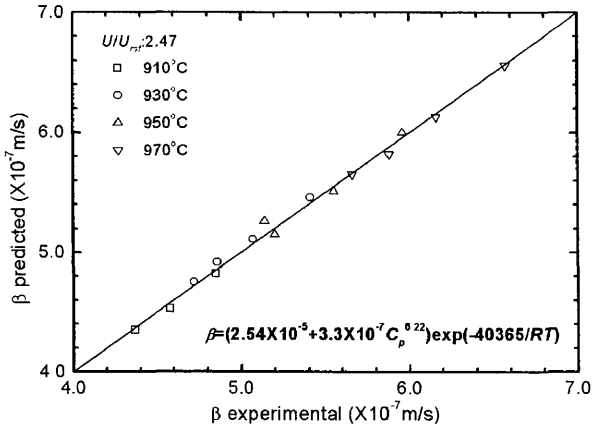

Fig. 7. Correlation of temperature, C_p and β.

A higher carbon transfer coefficient is found when the carburising is carried out in fluidised beds, compared with conventional gas methods. For example, carbon transfer coefficients of 1.25×10^{-7} m/s for an endothermic gas consisting of methane/propane up to 2.5×10^{-7} m/s for undiluted decomposed alcohols at the temperature of 900°C have been reported.[4,20] For direct-feed atmospheres using natural gas and air, or propane plus air, β was calculated in the range of 1.30 to 1.34×10^{-7} m/s.[4] In the present work the carbon transfer coefficient in fluidised bed is 2–4 times faster than that in a conventional carburising furnace due to the motion of gases and the fluidising medium in the fluidised bed.

The motion of the gas atmosphere and the fluidising medium is a decisive factor and facilitates the carbon transfer on the workpiece surface when the carburising process is performed in a fluidising bed. Their turbulence promotes the access of carburising gases (CH_4, CO) to the steel surface, the removal of products (H_2O, CO_2), which reduce the carbon potential of the atmosphere, and the access of fresh reactant. The thickness of the species boundary layer will be decreased and the difference of carbon potential

($C_p - C_p'$) will also decrease. Meanwhile, with high heat capacity of the fluidising medium is also a heat carrier. It not only compensates the energy loss resulting from the thermal dissociation and absorption of carburising gases on the steel surface, but also accelerates the thermal decomposition of hydrocarbons and reactions inside the species boundary layer. Simultaneously, the particles with high momentum, which is proportional to their density and velocity, provide a driving force to carry the carburising gases to the workpiece surface for absorption through the Nernst layer. Moreover, the fluidising medium sweeps the workpiece surface with a turbulent motion and continually removes the soot deposited on the workpiece surface. This promotes the absorption ability of the surface layer and, simultaneously, enables the access of fresh gas carrying atoms of carbon for diffusion. These factors directly affect the carbon transfer. In contrast, during a conventional gas carburising process, the access of CO and CH_4 to the workpiece surface and the removal of CO_2 and H_2O from the boundary layer only depends on the sweeping of the workpiece surface by gases.

5.2. Fluidising Velocity

Figure 8 shows the effect of fluidising velocity on the carbon transfer coefficient. It also shows the carbon transfer coefficients for the carburising process with carbon potential of 1.46% at a bed temperature of 930°C, and with the carbon potential of 1.38% at a bed temperature of 950°C, to compare β at a constant carbon potential or bed temperature. The rate of carbon transfer at the workpiece surface is increased by increasing the fluidising velocity. The increase in fluidising velocity results in an increase in the diffusion of gases and a decrease in the boundary layer, as well providing more fresh carburising gases. Simultaneously, the soot deposited on workpiece surface is subject to more rapid sweeping, because of the high frequency of bubbles and the momentum of the particles. The high heat transfer rate resulting from a high fluidising velocity causes rapid heating of the atmosphere gases. This generates the conditions for accelerated thermal decomposition of the hydrocarbons in the fluidised bed and the dissolution and absorption of carburising gases on the workpiece surface. Therefore, β increases with an increase in the fluidising velocity.

However, a decrease was found as the fluidising velocity increased beyond a critical value. The maximum carbon transfer coefficient occurs at the fluidising number, U/U_{mf}, of about 2.5–3.0. This can be attributed to the dynamic characteristics of two-phase flow in the bubble-fluidised bed. The bubble and emulsion phases periodically sweep the workpiece surface. With an increase in the fluidising velocity, it is proposed that the fraction of bubbles attaching to the workpiece surface increases, the fraction of emulsion decreases, and the effect of the particles in enhancing the carbon transfer decreases. Moreover, it is proposed that the high fluidising velocity results in high momentum of any given particle, which breaks the condition of absorption of carburising gases (CO and CH_4) on workpiece surface, inducing a decrease in the carbon transfer coefficient. Based on the motion characteristics of the gas and solids at the immersed surface in fluidised beds, the bubble and gas–solid emulsion phases alternately contact the immersed surface. The carbon transfer in the species boundary layer consists of emulsion and gas convections. Then the total mass flux from bed to an immersed surface is given by:

$$J = J_e(1-f_B) + J_B f_B \quad \text{.....(18)}$$

Because of the low diffusion coefficient of the carburising gases in the boundary layer and the low fraction of bubbles, the contribution of the bubbles to carbon transfer is relatively small and the carbon transfer is mainly from the emulsion phase, and consequently, Eq. (13) can be simplified to

$$J = J_e(1-f_B) \quad \text{.....(19)}$$

From the mass fluxes identified above, and considering the effect of carbon potential and bed temperature on carbon transfer coefficient then, accordingly, the total carbon transfer coefficient can be defined as

$$\beta = \beta_0 \beta_e (1-f_B) \quad \text{.....(20)}$$

where, β_0 is determined by Eq. (17). For the current experiment, β_0 is,

$$\beta_0 = (2.54\times10^{-5} + 3.3\times10^{-7} C_p^{6.22}) \exp\left(-\frac{40\,365}{RT}\right) \quad \text{.....(21)}$$

The carbon transfer coefficient in the emulsion phase, β_e, is determined by the following dimensionless equation, based on the theory of convective mass transfer, and the above hypothesis in explaining the variation of the carbon transfer coefficient with fluidising velocity.

$$Sh = \xi Re_e^n Sc^m (1-\alpha) \quad \text{.....(22)}$$

where

$$\alpha = \exp\left(-\frac{Q}{\rho_p (U-U_{mf})^2}\right)$$

In Eq. (22), the term $Re^n Sc^m$ presents the kinetic characteristics, carburising gas and fluidising medium properties and mass transfer, whereas, the term $1-\alpha$ indicates the effect of particle kinetic energy on reducing the carbon transfer rate, because the particle with a high kinetic energy breaks the absorption condition of the carburising gases. Summing Eqs. (20) and (22), then, the carbon transfer coefficient can

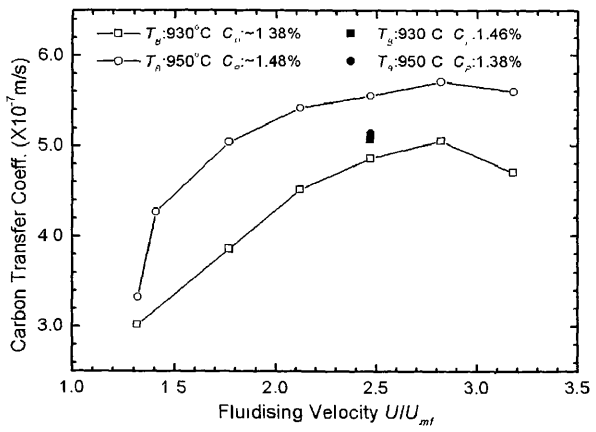

Fig. 8. Variation of β with U/U_{mf}.

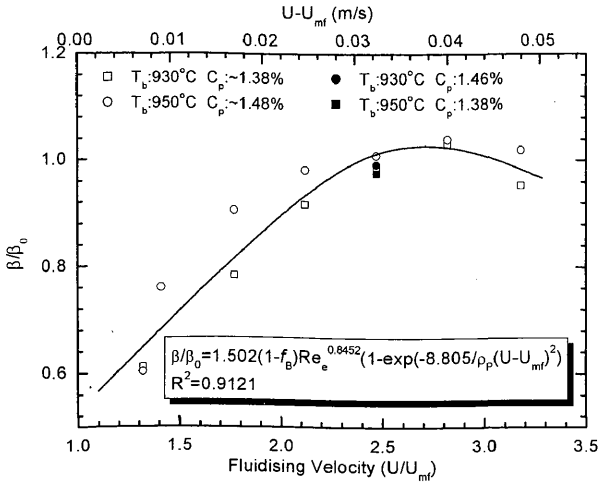

Fig. 9. Variation of β/β_0 with U/U_{mf} or $U-U_{mf}$.

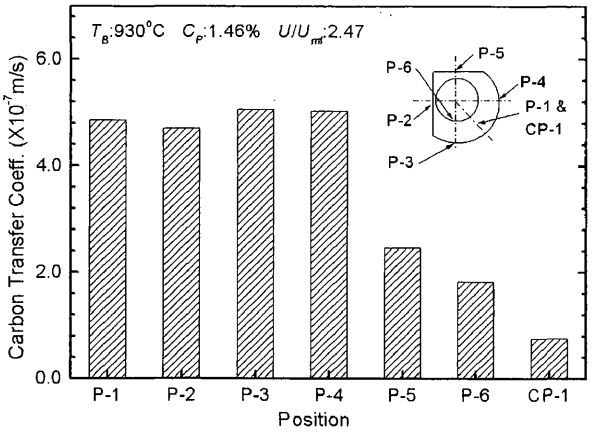

Fig. 10. Measured β over the workpiece surface (CP-1 corresponds to the adjacent surface of impacted workpiece).

be calculated by

$$\beta = \beta_0(1-f_B)\xi \frac{D_g}{d_p} \mathrm{Re}_e^n \mathrm{Sc}^m(1-\alpha) \quad \text{.....(23)}$$

To determine the parameters in Eq. (17), a sub-coefficient of carbon transfer, β/β_0, which does not change with the carbon potential and temperature for a given fluidising velocity, was introduced. The parameters obtained in the current work are given in Eq. (24) and shown in **Fig. 9**.

$$\beta = 1.5022\beta_0(1-f_B)\frac{1}{d_p}\mathrm{Re}_e^{0.8452}(1-\alpha) \quad \text{.....(24)}$$

where

$$\alpha = \exp\left(-\frac{8.805}{\rho_p(U-U_{mf})^2}\right)$$

The result shown in Eq. (24) is based on only the limited experiment data and only fluidising velocity was varied in the measurement. However, there are many other parameters, such as diameter and shape of the particles, physical properties of carburising gases and the fluidising medium, the mass diffusion coefficient of the species in the carburising atmosphere and the size of immersed object and fluidised bed. All of these parameters affect the carbon transfer in fluidised bed significantly. Therefore, it is necessary to carry out further experimentation to validate Eq. (24).

5.3. Local Carbon Transfer Coefficients around the Workpiece

Figure 10 shows a typical result of the carbon transfer coefficient at different position of workpiece. It can be seen that the carbon transfer at the positions (P-1, P-2, P-3 and P-4), where the particles are fluidised, is higher than that at positions (P-5 and P-6) where the particles are hardly moving. The lowest carbon transfer was measured at the position (CP-1), where adjacent surface of workpieces were in contact with each other. Comparing β at the fluidisation points (P-1–P-4), the carbon transfer coefficients at the curved surfaces (P-3 and P-4) are a little higher than that at vertical surfaces (P-1 and P-2), because of the stronger vertical momentum of particle flowing upward with fluidising gas. The result can also be seen in Figs. (11(a)) and (12(a)), comparing β at the curved surfaces ($-90°$, $-55°$, $-30°$, $0°$, $30°$, $60°$) with vertical surface ($180°$). The results from all the experiments clearly show that the carbon transfer coefficients at P-1 and P-2, which are on the vertical surface, are approximately same.

For the stagnation points, P-5 and P-6, there is no affect of particle motion on the carbon transfer. In fact, the carbon transfer in the two points is similar to that previously mentioned for a conventional carburising gas furnace. The process of access of CO and CH_4 to the workpiece surface and the removal of CO_2 and H_2O from the boundary layer occurs by diffusion in the gases between the stagnant particles and washing by fresh carburising gases flowing through stagnation layer. The lower carbon transfer coefficients at P-6 compared with P-5 further shows the effect of particle stagnation on carbon transfer. There is expected to be less movement of particles at the internal surface (P-6) than the external surface (P-5). Because the carburising gas flows slowly between stagnant particles, there is a thick species boundary layer through which the carburising atmosphere moves away from workpiece surface. The energy loss caused by thermal dissociation and absorption of the carburising gas cannot be compensated for, because of the low heat transfer rate through the stagnation particle layer and the high heat of chemical absorption. Generally the heat of chemical absorption is 160–400 kJ/mol, which is of the same order of magnitude as the heat of the chemical reaction. Compared with the conventional carburising methods, the carburising conditions at the stagnant particle layer when the process is performed in fluidised beds are more adverse. The carbon transfer coefficients will decrease with an increase in the thickness of stagnation particle layer. Therefore, a low carbon transfer coefficient was found at the upper stagnation positions on the outside and inside workpiece surfaces, and for some cases it is even less than 1.5×10^{-7} m/s, which is a typical value of the carbon transfer coefficient in the conventional carburising furnaces. The carbon transfer coefficients at the fluidisation points is 2–4 times higher than that at the stagnation points. This difference around the part is an important practical issue and suggests more attention is required for big workpiece to be carburised in fluidised beds. Less variation around the part is expected in conventional gas-carburising furnaces.

Figures 11 and **12** show the carbon transfer coefficients on the outside (a) and inside (b) semi-circumferential work-

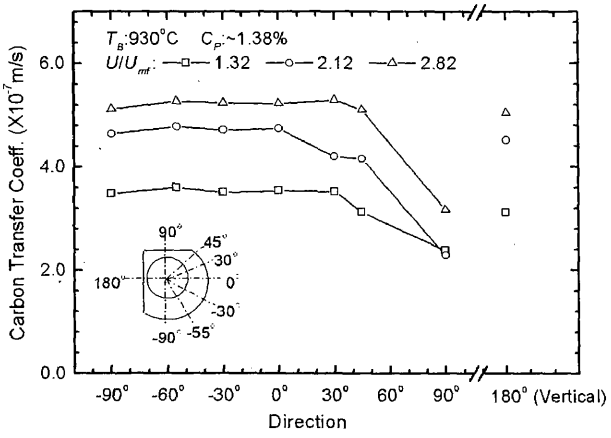

(a) On outside surface

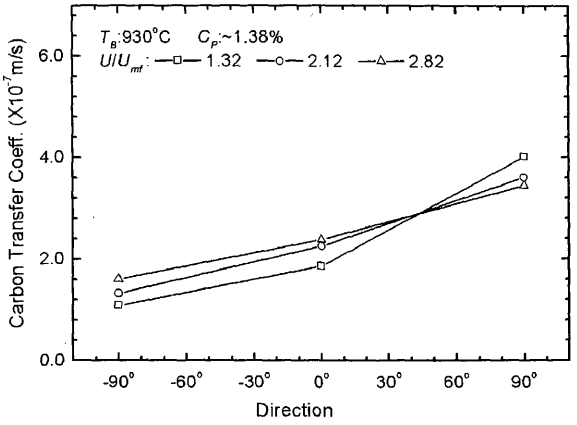

(b) On inside surface

Fig. 11. Variation of β with position.

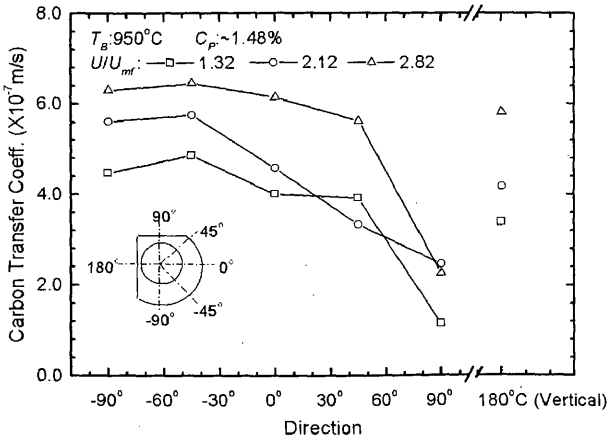

(a) On outside surface

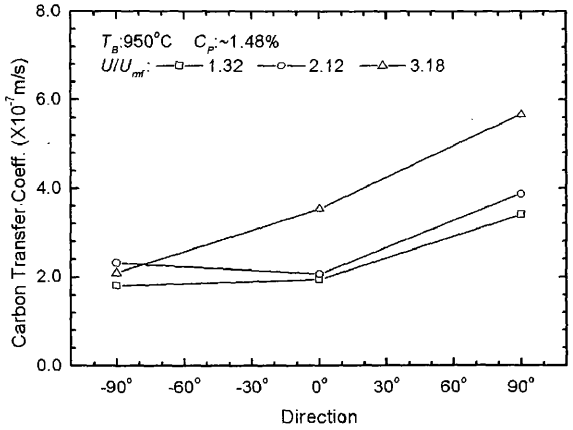

(b) On inside surface

Fig. 12. Variation of β with position.

piece surface at the conditions of fluidising velocity of $1.32U_{mf}$, $2.12U_{mf}$ and $2.82U_{mf}$, for the carburising processes performed in a fluidised bed with a temperature of 930°C and an averaged carbon potential of 1.38%, and in a fluidised with a temperature of 950°C and an averaged carbon potential of 1.48%, respectively.

The maximum carbon transfer coefficient is found at the angular position of −60°–−45° on outside surface. A rapid decrease in carbon transfer coefficients occurs from 45°. The lowest is at the upper point (90°) because of the stagnation of particles on the upper plane of the workpiece. This agrees with the results of other similar heat transfer experiments, and also is in agreement with the momentum distribution around the workpiece. Theoretical and computational results of the variations of Re_D around a bar with diameter of 80 mm immersed in a vessel with width of 200 mm is shown in **Fig. 13**. The complex flow of dense gas solid two-phase in fluidised bed was simplified to a gas–solid emulsion phase flowing in vessel, because there is not any accepted theory applied in density two-phase flow. Figure 13 shows that the position of maximum Re_D is 62° (248° symmetrically) operating at a velocity of $2.27U_{mf}$ and moves to a high angular position with an increase in velocity. A high Re_D means a high force or momentum acting on the workpiece surface, resulting in a high carbon transfer rate. The momentum boundary layer begins to move out of the surface at the position of 50° (130° symmetrically). Then the fluidising particles may stagnate on the upper surface of

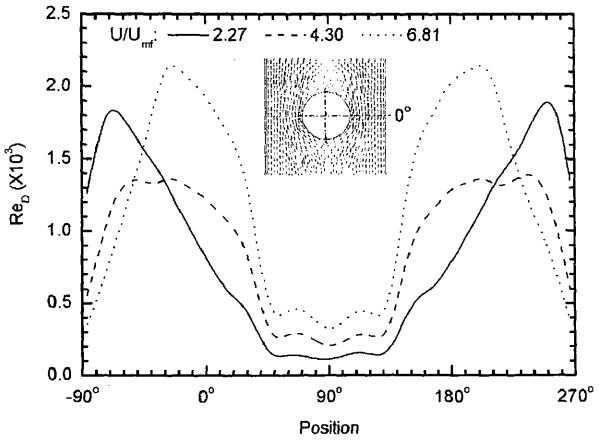

Fig. 13. Re distribution around a bar.

50°–130°. The thickness of the stagnant particles layer, which significantly reduces the carbon transfer rate, increases as the position rises along the sample surface.

The carbon transfer coefficients depend on the flow characteristics of the carburising gases besides the behaviour of particles. In the inside space of the workpiece, the velocity of gases is reduced, and an eddy with low velocity is formed, because the gases are shadowed by the workpiece body. The carbon transfer at the position of −90° on the inside surface is lower than at the position of 90° on outside surface, because the former position is in the shadow, although both positions contact the stagnation particle layer.

The same reason results in a lower carbon transfer coefficient at the position of 90° on the inside surface than at the position of −90° on the outsider surface, near both positions the particles are fluidised. Because of the very low flow of the carburising gases between workpieces immersed in the fluidised bed, the insufficient of the fresh carburising gases resulted in a lowest carbon transfer coefficient in the all measurement shown in Fig. 10. For the inside surfaces shown in Figs. 11(b) and 12(b), the lower carbon-transfer coefficient at −90° compared with that at 0° is caused by the higher thickness of the stagnant particle layer and the lower velocity of gases, the higher carbon-transfer coefficient at 90° than at 0° is from a higher gas velocity and without a stagnation particle layer at the former position. The thickness of stagnation particle layer and the flow of carburising gases are determined by the configuration of workpiece. Therefore, a low carbon transfer rate will be at the shadowed surface of workpiece with a deep hole inside, when the carburising process is performed in fluidised beds. Thus it is significant to orient the workpiece carefully in fluidised beds.

6. Conclusions

The transfer of carbon to an immersed workpiece surface in fluidised beds is much higher than that in conventional gas carburising furnaces. The motions of gas–solid emulsion and bubble phases in fluidised beds significantly intensify the diffusion of species in the boundary layer, enhancing activation and absorption of carburising gases on the workpiece surface. The fluidising velocity is important on affecting carbon transfer. Exceeding fluidising velocity reduces the carbon transfer in fluidised bed.

Analysis of the results leads to the following empirical relationships between the carburising parameters and carbon transfer coefficient:

$$\beta = 1.5022\beta_0(1-f_B)\frac{1}{d_p}\mathrm{Re}_e^{0.8452}(1-\alpha)$$

$$\beta_0 = (2.54\times10^{-5}+3.3\times10^{-7}C_p^{6.22})\exp\left(-\frac{40\,365}{RT}\right)$$

$$\alpha = \exp\left(-\frac{8.805}{\rho_p(U-U_{mf})^2}\right)$$

The remarkable variation in the values of the carbon transfer coefficient at different position on surface was found. The stagnation particle layer formed on the workpiece surface reduces the carbon transfer. The precise orientation of workpiece loaded in a fluidised bed is critical for the effective formation of a uniform case in the workpiece.

Acknowledgment

The authors would like to thank John Whales, Geoffery Giles, Steven Eden and Saeid Nahavandi in the School of Engineering and Technology at Deakin University for their assistance during the experimentation.

Nomenclature

a_1, a_2: Constants in Eq. (17)
a_g: Carbon activity of carburising gases
a_c: Carbon activity in steel
C: Carbon content
C_0: Carbon content in steel core
C_p: Carbon potential of carburising gases
d_p: Diameter of fluidising medium
D: Diffusivity of carbon within steel
D_g: Diffusivity of carbon in gases
f_B: Bubble fraction on immersed surface
J: Mass transfer flux
k_f: Forward equilibrium constant of reaction i
k_i: Backward equilibrium constant of reaction i
K_i: Equilibrium constant of reaction i
P: Fractional pressure of gas
Q: Activation energy
R: Universal gas constant
Re: Reynolds number
Sc: Schmidt number
Sh: Sherwood number
T: Temperature
t: Carburising time
U: Fluidising velocity
U_{mf}: Minimum fluidising velocity
x: Depth from steel surface

Greek symbols
α: Defined by Eq. (22)
β: Carbon transfer coefficient
ρ_p: Density of fluidising medium
ν: Rate of chemical reaction
ξ: Constant in Eq. (22)

Superscripts and subscripts
B: Bubble
e: Emulsion phase
m, n: Constant

REFERENCES

1) R. W. Reynoldson: *Heat Treat. Met.*, **7** (1980), 35.
2) T. Fukuda and H. Hattori: *Heat Treat. Met.*, **15** (1988), 53.
3) R. W. Reynoldson: 17th ASM Heat Treating Society Conf. Proc. the 1st Int. Induction Heat Treating Symp., ASM International, Ohio, (1997), 53.
4) B. Edenhofer: *Heat Treat. Met.*, **22** (1995), 55.
5) J. Jasinski, L. Jeziorski and M. Kubara: *Heat Treat. Met.*, **12** (1985), 42.
6) K. E. Moore and D. N. Collins: *Heat Treat. Met.*, **23** (1996), 95.
7) L. Multak: 17th ASM Heat Treating Society Conf. Proc. the 1st Int. Induction Heat Treating Symp., ASM International, Ohio, (1997), 121.
8) M. Glasser: *Adv. Mater. Process.*, **153** (1998), 84MM.
9) J. Rawers, T. Wang, R. Krabbe and S. Kimura: *J. Mater. Synthesis Processing*, **3** (1995), 393.
10) R. W. Reynoldson: *Materials Australia*, (1999), May/June, 25.
11) D. Zhang and A. Yang: *Heat Treat. Met. (China)*, (1991), 37.
12) D. Dragomir and L. Druga: *Mater. Sci. Eng. A*, **302** (2001), 115.
13) P. J. Meschter and H. J. Grabke: *Metall. Trans.*, **10** (1979), 323.
14) J. H. Kaspersma and R. H. Shery: *Metall. Trans.*, **12B** (1981), 77.
15) R. J. Fruehan: *Metall. Trans.*, **4** (1973), 2123.
16) G. P. Ling and Z. Y. Ma: *Heat Treat. Met. (China)*, (2000), 36.
17) H. J. Grabke: *Metall. Trans.*, **1** (1970), 2971.
18) D. Geldart: *Powder Technol.*, **7** (1973), 285.
19) F. P. Incropera and D. P. DeWitt: Fundamentals of Heat and Mass Transfer, John Wiley & Sons Inc., New York, (1996), 239.
20) G. E. Totten and M. A. H. Howes: Steel Heat Treatment Handbook, Marcel Dekker, Inc., New York, (1997).
21) F. Neumann and U. Wyss: *Härt-Tech. Mitt.*, **25** (1970), 253.